ELSEVIER

Thermochimica Acta 287 (1996) 111–129

thermochimica acta

Mössbauer spectroscopic and thermal decomposition studies of alkylamine and nitrogen heterocyclic substituted pentacyanoferrate(II) complexes

R.B. Lanjewar [1], S. Kawata [a], T. Nawa [a], S. Kitagawa [a], A.N. Garg [b], M. Katada [a,*]

[a] *Radioisotope Research centre, Tokyo Metropolitan University, Minami osawa, Hachioji, Tokyo 192-03 Japan*

[b] *Department of Chemistry, Nagpur University, Nagpur, 440 010, India*

Received 24 January 1996; accepted 19 March 1996

Abstract

Substituted pentacyanoferrate(II) complexes $Na_3[Fe(CN)_5L]\cdot xH_2O$ have been obtained for di-*sec*-butylamine, tri-*n*-amylamine, pyrazole, pyrazine, pyrrole, and 2-,3- and 4-cyanopyridine. Microanalysis, UV-visible, infrared, and Mössbauer spectroscopies, TGA–DTG and XRD were used to characterize the complexes. Each complex has an absorption band in the visible region that is assigned to a d–d transition. Mössbauer parameters are used to classify the various ligands according to their σ- and π- bonding abilities. The Mössbauer spectra of these complexes exhibit a quadrupole doublet, $\Delta E_Q = 0.71$–0.84 mm s^{-1} at room temperature. The isomer shift (δ) values fall within 0.00 ± 0.02 mm s^{-1} which suggests that the iron atom is in a +2 low-spin state. Thermolysis of the solids leads to water release, ligand release and/or decomposition, yielding elemental metal, metal carbides, haematite and magnetite.

Keywords: Thermal decomposition; Mössbauer spectroscopy; Pentacyanoferrates(II); Iron(I) complex

1. Introduction

Substantial interest in substituted pentacyanoferrates(II) continues. A wide variety of substituted pentacyanoferrates(II) have been synthesized and extensively studied by

* Corresponding author.

[1] On leave from A.N. College, Anandwan 442 914, India.

PII: S0040-6031(96)02989-9

Mössbauer [1–3], NMR [4, 5]and X-ray photoelectron spectroscopy [6, 7]. De Araujo and coworkers [3, 8] rationalized the linear correlation of Mössbauer parameters on the basis of $\sigma-\pi$ interactions of the ligands. Earlier, we studied several alkyl- and arylamine–substituted pentacyanoferrate(II) complexes [9–11]. Recently, special attention has been given to the study of the interaction of iron with ligands of biological importance [8,12], and the thermal behaviour of simple and complex cyanides has been the subject of much work. The decomposition has been shown to involve cyanogen release, usually with nitrogen evolution and formation of metal carbides[13–17]. Brar and Varma [16] studied the thermal decomposition products of sodium pentacyanoferrate(II) using Mössbauer spectroscopy. Sileo et al. [17] investigated the thermal behaviour of pentacyanoligand-ferrate(II) complexes, with L being pyrazine and pyridine, and proposed water release, finally yielding metal carbide.

In the present communication, we report the synthesis of substituted pentacyanoferrate(II) complexes, $Na_3[Fe(CN)_5L]\cdot xH_2O$ where L is di-*sec*-butylamine (di-*s*-Bu), tri-*n*-amylamine (tri-*n*-Am), pyrazine (PYZN), pyrazole (PYZL), pyrrole (PYRL), 2-cyanopyridine (2-CNPy), 3-cyanopyridine (3-CNPy) and 4-cyanopyridine (4-CNpy). The complexes have been characterized by elemental analysis, UV-visible, infrared, and Mössbauer spectroscopy, and XRD. An attempt has been made to identify the thermal decomposition of the intermediate and final products of pentacyanoferrates by employing TGA, DTG, XRD and Mössbauer spectroscopy.

2. Experimental

All reagents used were of AR, GR or high-purity grade. The complexes were prepared by modifying the procedure adopted by Manoharan and Fanning [2].

2.1. Preparation of the complexes

A solution containing 0.47 g of hydroxylamine hydrochloride and 0.54 g of NaOH in 20 ml water was prepared. Then either 10 ml of the respective amine or 10 ml of 10% heterocyclic ligand in ethanol was added. The mixture was kept on ice for 1 h and then added dropwise to an ice-cold solution of 2 g sodium pentacyanoitrosylferrate(II) in 20 ml water. In each case, an oily layer separated after adding cold alcohol. The complexes were forced to solidify by thorough washing with absolute ethanol and then drying for 24 h over concentrated H_2SO_4 in a desiccator.

The complexes were characterized by elemental analysis (C, H, and N). The water molecules were adjusted according to the molecular formula.

2.2. Physical measurements

Mössbauer spectra were recorded on a transducer-driven Mössbauer spectrometer in constant acceleration mode (ELCIENT) at room temperature. A $\sim$ 5m Ci^{57} Co(Rh) source was used. The spectrometer was calibrated using natural iron foil. All isomer

shift values were referred to the metallic iron. The spectra were fitted Lorentzian lines. Mössbauer spectra of the thermal decomposition products were recorded after heating the complexes at different temperature in an N_2 atmosphere in a muffle furnace for 3 h and quenching to room temperature. UV-visible spectra of the pentacyanoferrate(II) complexes were recorded in aqueous solution using a Hitachi model U-3500 spectrophotometer and a 1-cm path length. Infrared spectra were obtained on a sample in KBr pellets using a Hitachi Nicolet model I-5040 FTIR spectrophotometer. Thermogravimetric (TGA–DTG) studies were carried out in N_2 atmosphere using a Seiko Instrument Inc. SSC/5200 at a heating rate 10°C min^{-1}. XRD of the decomposition products were recorded using an MAC science MXP-18 automated diffractometer using Cu Kα radiation.

3. Results and discussion

All the complexes are coloured, solid and stable under normal atmospheric conditions. Analytical data, electronic spectral bands and characteristic IR frequencies due to $\nu(C \equiv N)$, $\delta(Fe–CN)$ and $\nu(Fe–C)$ are listed in Table 1. Mössbauer spectra of all the complexes exhibit a well-resolved quadrupole doublet at room temperature. Typical Mössbauer spectra of di-*sec*-butylamine, tri-*n*-amylamine, pyrazole, pyrrole and pyrazine-substituted pentacyanoferrate(II) complexes at room temperature and after heating at different temperature are shown in Figs. 1, 2, 3, 4 and 5 respectively. Mössbauer parameters at room temperature and different temperatures are listed in Table 2. TGA and DTG plots of pyrazole, pyrrole and pyrazine-substituted pentacyanoferrates(II) are shown in Fig. 6. Their respective thermogravimetric data are listed in Table 3.

3.1. Electronic spectra

Aqueous solutions of pentacyanoferrates(II) were found to be pale yellow, exhibiting an absorption in the UV-visible region. These bands are shown along with data for substituted pentacyanoferrate(II) complexes in Table 1. In d^6 pentacyanoferrates(II) of C_{4v} symmetry for which the ground state is $^1A_1$, the low-energy excited states of the same multiplicity are $^1A_2$ and $^1E(1)$ [18]. Thus two d–d transitions are typically observed for such complexes: $^1E(1) \leftarrow {}^1A_1$ and $^1A_2 \leftarrow {}^1A_1$. The first band which has energy and intensity considerably greater than the second has been assigned to the $^1E(1) \leftarrow {}^1A_1$ transition. The second, a weak band, occurred at lower energies and should be relatively insensitive to the ligand L. The $^1A_2 \leftarrow {}^1A_1$ is expected at 31,000 cm^{-1} but it is not observed due to the electron transfer band in that region. The $^1E(1) \leftarrow {}^1A_1$ transition can be observed for the pentacyanoferrate(II) complexes in the region 22500–37900 cm^{-1} [19]. By analogy, considering its energy and intensity, the band due to $^1E(1) \leftarrow {}^1A_1$ in pentacyanoferrates(II) is found in the region 23,800–29,900 cm^{-1}. As the d–d bands have a large and asymmetric form (Fig. 7), we suggests that $^1A_2 \leftarrow {}^1A_1$ transitions occur superimposed on $^1E(1) \leftarrow {}^1A_1$ in the spectra of the studied complexes.

Table 1
Analytical data, IR frequencies and electronic spectral bands for substituted pentacyanoferrates(II)

Complex	Found (Calc.)			IR frequencies/ cm^{-1}			Electronic spectral band/ cm^{-1}
	%C	%H	%N	ν(CN)	δ(FeCN)	ν(Fe–C)	
1 $Na_3[Fe(CN)_5\{(s\text{-}C_4H_9)_2NH\}]\cdot 3H_2O$	34.65 (35.68)	5.63 (5.49)	20.88 (19.21)	2045s 2015m	570m	430s	25,000
2 $Na_3[Fe(CN)_5\{(n\text{-}C_5H_{11})_3N\}]\cdot 7H_2O$	38.97 (39.45)	7.49 (7.72)	13.92 (13.82)	2045s, 2015w	575s	430w	25,000
3 $Na_3[Fe(CN)_5C_3H_4N_2]\cdot 3H_2O$ (Pyrazole)	25.13 (25.46)	2.58 (2.60)	26.03 (25.99)	2050s	580s	410w	25,800
4 $Na_3[Fe(CN)_5(C_4H_4N_2)]\cdot 3H_2O$ (Pyrazine)	28.01 (27.76)	2.63 (2.57)	24.97 (25.19)	2090w, 2055s 2040vw	570s	430s	29,900
5 $Na_3[Fe(CN)_5C_4H_4N]\cdot 3.5H_2O$ (Pyrrole)	28.11 (28.19)	2.91 (2.87)	22.16 (21.93)	2046s,	570s	435w	25,500
6 $Na_3[Fe(CN)_5$2-CN-$C_5H_4N]\cdot 8H_2O$	26.14 (26.24)	4.11 (3.97)	19.64 (19.48)	2055s,	570m	430s	24,700
7 $Na_3[Fe(CN)_5$3-CN-$C_5H_4N]\cdot 3H_2O$	32.13 (31.96)	2.10 (1.85)	24.07 (23.72)	2090w 2045s 2010w	575m	455s	25,200
8 $Na_3[Fe(CN)_5$4-CN-$C_5H_4N]\cdot 4H_2O$	30.17 (30.62)	3.01 (2.78)	22.58 (22.74)	2080w 2046	575s	430vw	23,800

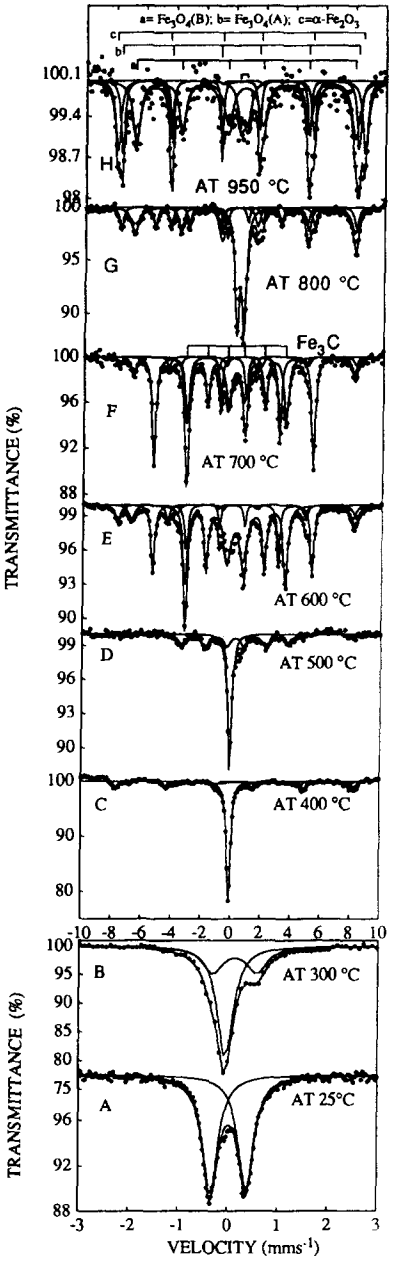

Fig. 1. Mössbauer spectra of di-s-butylamine-substituted pentacyanoferrate(II) complex at (A) room temperature and after heating at (B) 300°C, (C) 500°C, (D) 500°C, (E) 600°C, (F) 700°C, (G) 800°C and (H) 950°C for 3 h.

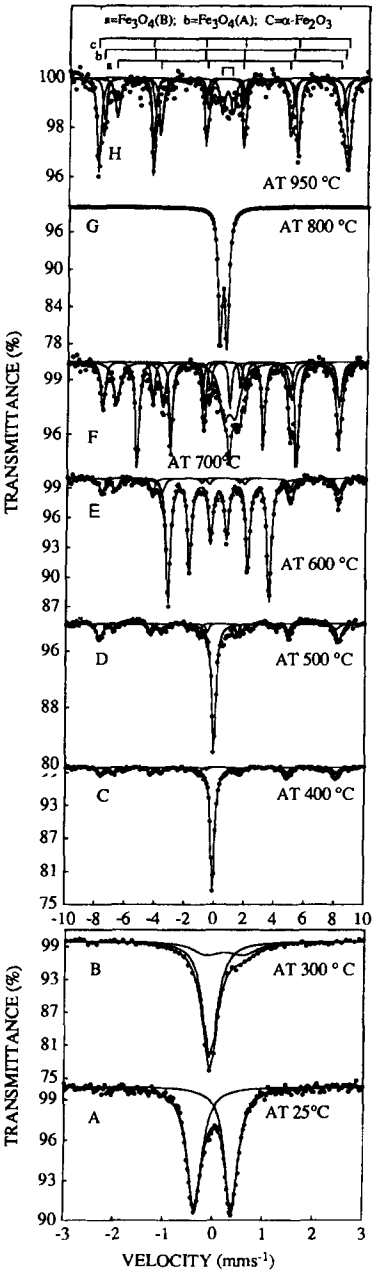

Fig. 2. Mössbauer spectra of tri-*n*-amylamine-substituted pentacyanoferrate(II) complex at (A) room temperature and after heating at (B) 300°C, (C) 400°C, (D) 500°C, (E) 600°C, (F) 700°C, (G) 800°C and (H) 950°C for 3 h.

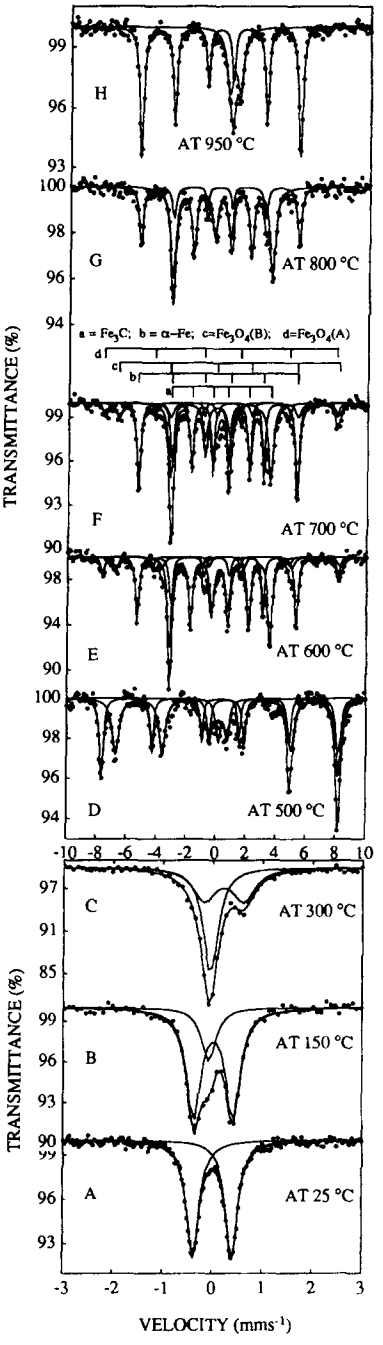

Fig. 3. Mössbauer spectra of pyrazole-substituted pentacyanoferrate(II) complex at (A) room temperature and after heating at (B) 150°C, (C) 300°C, (D) 500°C, (E) 600°C, (F) 700°C, (G) 800°C and (H) 950°C for 3 h.

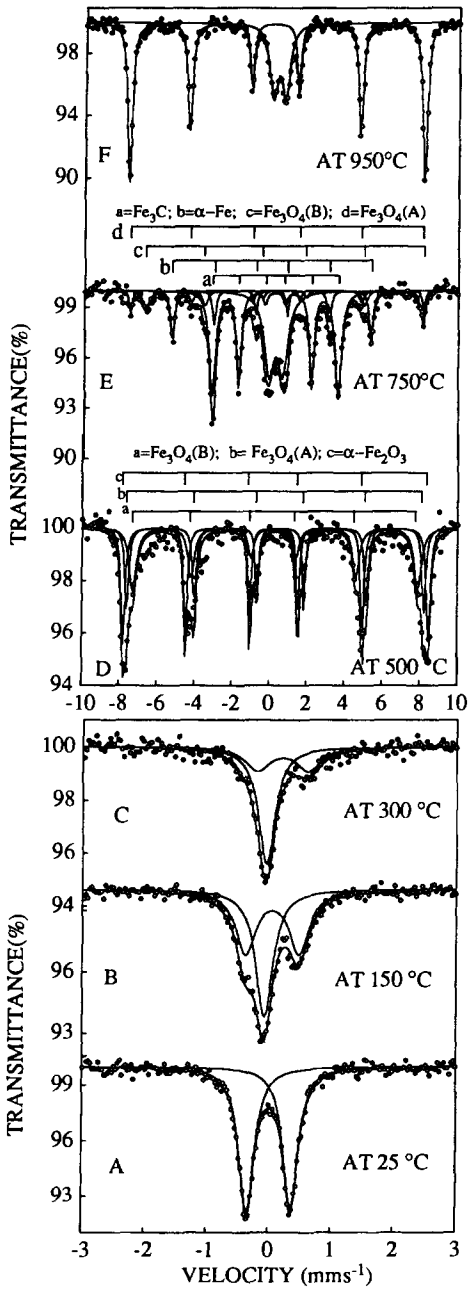

Fig. 4. Mössbauer spectra of pyrrole-substituted pentacyanoferrate(II) complex at (A) room temperature and after heating at (B) 150°C, (C) 300°C, (D) 500°C, (E) 750°C and (F) 950°C for 3 h.

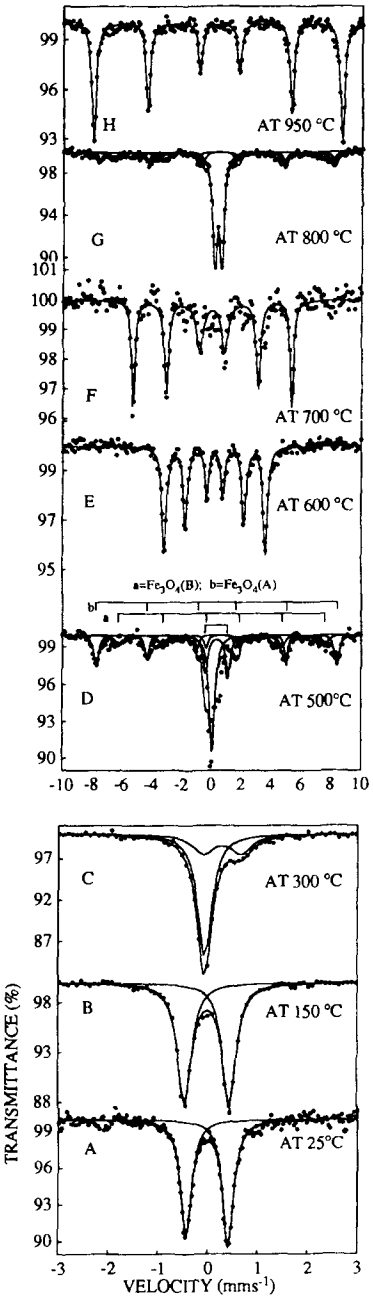

Fig. 5. Mössbauer spectra of pyrazine-substituted pentacyanoferrate(II) complex at (A) room temperature and after heating at (B) 300°C, (C) 400°C, (D) 500°C, (E) 600°C, (F) 700°C, (G) 800°C and (H) 950°C for 3 h.

Table 2
Mössbauer parameters for substituted pentacyanoferrate(II) and its thermal decomposition products

Complex $Na_3[Fe(CN)_5L]$ L =	Temp./ °C	Isomer shift δ/ mm s^{-1}	Quadrupole splitting, ΔE_Q/ mm s^{-1}	H_{eff}/ kOe	Possible products
(s-C_4H_9)$_2$NH	25	0.02	0.72	–	–
	300	0.13	0.89	–	–
		−0.05	–	–	–
	400	0.33	0.00	496	Fe_3O_4(A)
		0.55	0.14	457	Fe_3O_4(B)
		−0.07			
	500	0.25	0.04	220	Fe_3C
		−0.06	–		
	600	0.30	0.02	497	Fe_3O_4(A)
		0.59	0.09	460	Fe_3O_4(B)
		0.19	0.00	209	Fe_3C
	700	0.25	0.03	492	Fe_3O_4(A)
		0.68	−0.02	460	Fe_3O_4(B)
		0.00	0.02	333	α-Fe
		0.19	0.01	207	Fe_3C
	800	0.25	0.02	490	Fe_3O_4(A)
		0.65	0.00	459	Fe_3O_4(B)
		0.01	0.03	331	α-Fe
		0.37	0.46	–	α-$NaFeO_2$
	950	0.29	0.00	491	Fe_3O_4(A)
		0.62	0.02	458	Fe_3O_4(B)
		0.36	0.04	515	α-Fe_2O_3
(n-C_5H_{11})$_3$N	25	0.00	0.74	–	–
	300	0.22	0.74	–	–
		−0.07	–	–	–
	400	0.26	0.03	490	Fe_3O_4(A)
		0.63	−0.01	458	Fe_3O_4(B)
		−0.07	–	–	
	500	0.26	0.06	497	Fe_3O_4(A)
		0.65	−0.02	461	Fe_3O_4(B)
		−0.06	–	–	
	600	0.27	−0.04	491	Fe_3O_4(A)
		0.71	−0.02	465	Fe_3O_4(B)
		0.19	0.01	209	Fe_3C
	700	0.26	−0.03	491	Fe_3O_4(A)
		0.70	−0.02	462	Fe_3O_4(B)
		0.00	0.00	331	α-Fe
		0.85	0.73	–	–
	800	0.36	0.46	–	α-$NaFeO_2$
	950	0.38	0.13	520	α-Fe_2O_3
		0.37	0.02	501	Fe_3O_4(A)
		0.54	0.02	464	Fe_3O_4(B)
(PYZL)	25	0.01	0.78	–	–
	150	0.02	0.78	–	–
		−0.07	–	–	–
	300	0.22	0.79	–	–
		−0.04	–	–	–

Table 2 (*Continued*)

Complex $Na_3[Fe(CN)_5L]$ L =	Temp./ °C	Isomer shift δ/ mm s^{-1}	Quadrupole splitting, ΔE_Q/ mm s^{-1}	H_{eff}/ kOe	Possible products
		−0.07	–	–	–
	500	0.28	−0.04	493	Fe_3O_4(A)
		0.70	0.01	462	Fe_3O_4(B)
		0.44	0.58	–	
	600	0.19	0.00	209	Fe_3C
		0.00	0.00	331	α-Fe
		0.26	−0.07	490	Fe_3O_4(A)
		0.72	0.12	468	Fe_3O_4(B)
	700	−0.01	0.00	330	α-Fe
		0.18	0.01	208	Fe_3C
		0.20	−0.13	482	Fe_3O_4(A)
		0.72	−0.01	457	Fe_3O_4(B)
	800	0.18	0.00	207	Ee_3c
		−0.01	0.01	330	α-Fe
	950	0.00	0.00	330	α-Fe
		0.93	0.67	-	$Fe_{1-x}O$
(PYZN)	25	−0.01	0.84	–	
	150	−0.01	0.89	–	
	300	0.29	0.75	–	
		−0.06	–	–	
	500	0.32	−0.01	500	Fe_3O_4(A)
		0.69	−0.07	429	Fe_3O_4(B)
		0.34	1.51	–	
	600	0.19	0.01	208	Fe_3C
	700	0.00	0.01	330	α-Fe
	800	0.28	0.03	492	Fe_3O_4(A)
		0.62	0.03	457	Fe_3O_4(B)
		0.36	0.46	–	–
	950	0.40	−0.13	517	α-Fe_2O_3
PYRL	25	−0.01	0.71		
	150	0.06	0.85	–	
		−0.07	–	–	–
	300	0.22	0.82	–	
		−0.04	–	–	–
	500	0.39	0.08	515	α-Fe_2O_3
		0.46	0.27	492	Fe_2O_3
		0.27	0.09	471	–
	750	0.30	0.02	488	Fe_3O_4(A)
		0.70	0.12	459	Fe_3O_4(B)
		0.22	0.00	209	Fe_3C
		0.03	0.00	331	α-Fe
		0.26	0.73	–	
	950	0.22	0.10	492	γ-Fe_2O_3
		0.37	0.65		α-$NaFeO_2$
2-CNPy	25	−0.01	0.84		
	150	0.13	0.76	–	–
		−0.06	–	–	–
	300	0.26	0.72	–	–

Table 2 (*Continued*)

Complex $Na_3[Fe(CN)_5L]$ L =	Temp./ °C	Isomer shift δ/ mm s^{-1}	Quadrupole splitting, ΔE_Q/ mm s^{-1}	H_{eff}/ kOe	Possible products
		−0.07	–	–	–
	500	0.30	0.02	501	Fe_3O_4(A)
		0.65	0.01	457	Fe_3O_4(B)
		0.19	0.00	209	Fe_3C
		−0.05	–	–	–
	750	0.02	0.00	330	α-Fe
		0.19	0.01	208	Fe_3C
	950	0.34	0.11	493	Fe_3O_4(A)
		0.64	0.00	437	Fe_3O_4(B)
		0.03	0.06	318	α-Fe
		0.93	0.81		$Fe_{1-x}O$

Errors in δ and ΔE_Q values are ± 0.02 mm s^{-1} and for H_{eff}, ± 5 kOe.

Table 3
Thermogravimetric data for substituted pentacyanoferrates(II) $Na_3[Fe(CN)_5L]\cdot xH_2O$ complexes

Complex L	DTG peak/ °C	Decomposition process	Constant wt. temp./°C	Final weight/ %
$(s\text{-}C_4H_9)_2NH$	65, 125 560, 910	Fast, slow, slow, fast Four-stage	960	17.7
$(n\text{-}C_5H_{11})_3N$	85, 128, 614, 907	Fast, slow, slow, fast Four-stage	945	15.9
PYZL	83, 130, 248, 996	Fast, slow, slow, fast Four-stage	1020	18.5
PYZN	90, 231, 299, 235, 970	Fast, slow, slow, Fast, fast; five-stage	980	16.0
PYRL	50, 109, 501, 560, 936	Fast, slow, fast, slow, Fast; five-stage	950	24.1
2-CNPy	68, 602, 940	Fast, slow, fast Three-stage	950	16.3
3-CNPy	83, 116, 226, 551, 940	Fast, slow, fast, slow, Fast; five-stage	980	18.0
4-CNPy	75, 233, 358 511, 966	Fast, slow, slow, Slow, fast five-stage	950	18.8

3.2. *Infrared spectra*

Various vibrational modes were assigned by comparison with those of other substituted pentacyanoferrate(II) complexes [20–23]. The most intense band due to $\nu(C \equiv N)$ was observed in the range 2090–2010 cm^{-1}. Three modes have previously been observed for $\nu(C \equiv N)$ of some di- and trialkylamine-substituted pentacyanofer-

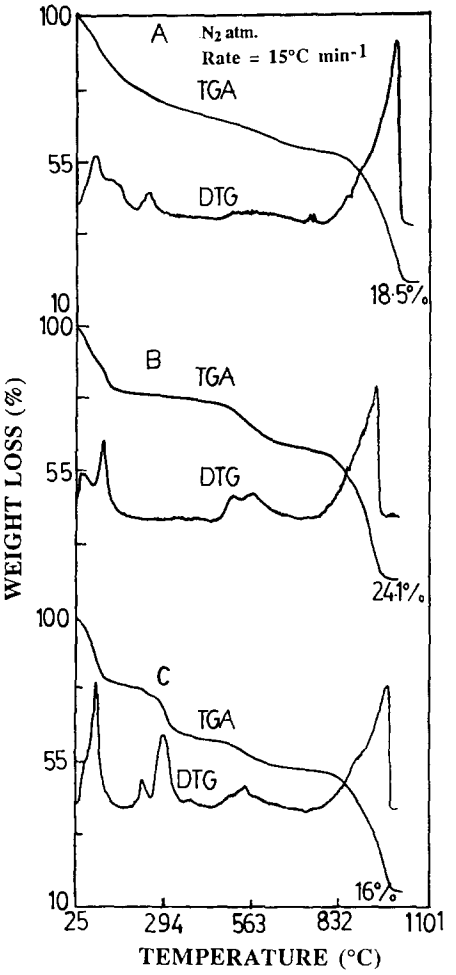

Fig. 6. Typical TGA and DTG plots of (A) pyrazole-, (B) pyrrole- and (C) pyrazine-substituted pentacyanoferrate(II) complexes.

rate(II) complexes [11]. Here, we observed two bands at $\sim$ 2045 and 2015 cm^{-1} for ν(C $\equiv$ N) in all substituted complexes, except for the pyrazine-substituted complex in which three bands at 2090, 2055 and 2045 cm^{-1} were observed. Another characteristic mode of medium intensity is due to δ(Fe–CN) observed at $\sim 565 \pm 10$ cm^{-1}. A very weak band observed at 430 ± 5 cm^{-1} has been assigned to ν(Fe–C) according to Fluck et al. [22]. The stretching mode Fe–N could not be assigned at this is expected to be observed at $\sim$ 250 cm^{-1}. An intense weak, broad peak in the region 3580–3405 cm^{-1} arose mainly due to weakly bonded water molecules in the lattice. The exact assignments of various bands in this region is not possible due to several overtone and combinations of bending vibrations. Similarly, a sharp to medium intense band at

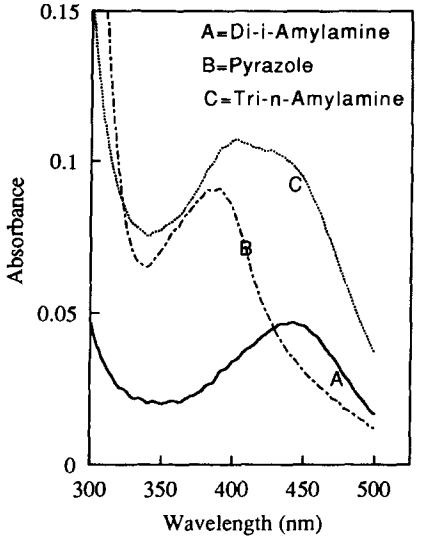

Fig. 7. Electronic spectra of (A) di-*n*-amylamine-, (B) pyrazole- and (C) tri-*n*-amylamine-substituted pentacyanoferrate(II) complexes.

$\sim 1600\ cm^{-1}$ has been assigned to the bending mode of H_2O. It may be noted that $\nu(C \equiv N)$, $\nu(Fe–C)$ and $\delta(Fe–CN)$ are unaffected by the substitution of alkylamine and heterocyclic ligands.

3.3. Mössbauer parameters

Room-temperature Mössbauer spectra of all the complexes exhibit a well-resolved quadrupole doublet with $\Delta E_Q = 0.70 - 0.83\ mm\ s^{-1}$ which indicates the presence of an electric field gradient with non-cubic symmetry at the Fe nucleus. The isomer shift δ reflects the changes in the electronic density at the Fe nucleus caused by modification in the electron populations of the valence orbital of the Fe atom. In pentacyanoferrate(II) complexes, the non-cubic electronic configuration of the central ion comes from the asymmetric σ- and π-bonding involving only the axial ligand L. The σ donation mechanism increase the s-electron population causing as increase in electron density at the Fe metal. The π mechanism decreases the shielding effects due to donation from the metal d-orbital to the ligand, causing an increase in the s-electron density. Therefore, the combined effect $(\sigma + \pi)$ increases the electron density at the Fe nucleus, thereby decreasing the isomer shift. Thus the values of δ are helpful to categorize the ligand L regarding its $(\sigma + \pi)$ bonding ability. For the case of iron compounds, the combined $(\sigma + \pi)$ effect increases with the decrease in isomer shift [24]. However, it is desirable to obtain information about the σ and π effects separately and this is possible simultaneously from the ΔE_Q and δ values. It can be seen from Table 4 that the combined $(\sigma + \pi)$ effect increases in the following order: H_2O < 4-CNPy < $(s\text{-}C_4H_9)_2NH$ < pyrazole < pyrrole < NH_3 < pyrazine < 3-CNPy < 2-CNPy < CN^- < CO < NO^+.

Table 4
Mössbauer parameters for pentacyanoferrate(II) complexes

$Fe(CN)_5L$ L =	ΔE_Q/ mm s^{-1}	δ (w.r.t.SNP)/ mm s^{-1}
NO^+	1.707	0.00
CO	0.366	0.118
CN^-	0.000	0.192
2-CNPy	0.839	0.258
3-CNPy	0.872	0.258
PYZN	0.842	0.262
NH_3	0.689	0.275
$(n\text{-}C_5H_{11})_3N$	0.742	0.276
PYZL	0.778	0.282
PYRL	0.708	0.281
$(s\text{-}C_4H_9)_2NH$	0.716	0.289
4-CNPy	0.804	0.294
H_2O	0.795	0.297

In pentacyanoferrate(II) complexes, the quadrupole splitting ΔE_Q is due to the ligand contribution and the aspherical electron distribution in the valence molecular orbital. The latter may arise due to anisotropic bond properties [25] as in the case of $[Fe(CN)_5L]^{3-}$. Here the metal-to-ligand bond is influenced by both σ and π interaction, and their relative strengths compared with CN^-. If L is a stronger donor than CN^-, $N(d_{z^2}) > N(d_{x^2-y^2})$ (where N represents the electron population in respective d orbitals) and a negative contribution of the valence molecular orbital $(V_{zz})_{MO}$ may result along M–L bond. However, if L is a more effective π-acceptor than CN^-, $N(d_{xy}) > [N(d_{xz}) + N(d_{yz})]/2$, because of a more pronounced charge delocalization from $M \rightarrow L$, i.e. $d_\pi \rightarrow p_\pi$, and a positive contribution to $(V_{zz})_{MO}$ is expected. The net effect is to make $(V_{zz})_{MO}$ more negative with increasing $(\sigma - \pi)$. The values of ΔE_Q listed in Table 4 show that the combined $(\sigma - \pi)$ effect increases in the following order: NO^+ < 3-CNPy < pyrazine ~ 2-CNPy < 4-CNPy < pyrazole < $(n\text{-}C_5H_{11})_3N$ < $(s\text{-}C_4H_9)_2NH$ < pyrrole < NH_3 < CO < CN^-.

3.4. *Thermal decomposition studies*

Several workers [14–17] have been able to identify successfully the different Fe species in iron complexes. Brar and Varma [16] and Sileo et al. [17] have studied the thermal decomposition behaviour of substituted pentacyanoferrate(II) complexes. Ganguli and Bhattacharya [26] proposed that Prussian blue exhibits semiconducting behaviour in the temperature range 30–150°C and three different stages of hydration. Inoue et al. [27] reported the thermal decomposition of Prussian blue and identified various products by Mössbauer spectroscopy.

A typical thermogram obtained in N_2 atmosphere is shown in Fig. 6. Dehydration, ligand L release, and cyanogen plus dinitrogen evolution occur in reasonably well-

resolved stages. Thermograms of substituted pentacyanoferrate(II) complexes are shown in Fig. 6. A perusal of the data in Table 3 suggests that all the complexes start decomposing at 50°C and yield a final stable product with 15.9–24.1% residual weight at 950–1000°C. In all cases, decomposition is multi-stage, as evidenced by the number of DTG peaks.

3.4.1. Di -s-*butylamine and tri* -n-*amylamine-substituted pentacyanoferrates (II)*

Thermograms of di-*s*-butylamine and tri-*n*-amylamine-substituted pentacyanoferrate(II) complexes show a multi-stage decomposition. In the first stage, rapid decomposition occurs around 100°C, in later stages, decomposition slows down, ultimately yielding stable end products at 950°C. For tri-*n*-Am- and di-*s*-Bu-substituted complexes, three sharp DTG peaks appear at 85, 140 and 930°C. In both cases, four-stage decompositions occur. In the first stage, water molecules are lost and cyanogen gas is probably released [11]. It is also possible that some interaction in the reaction vessel at higher temperature might have taken place [17].

Mössbauer spectra of di-*s*-butylamine and tri-*n*-amylamine-substituted pentacyanoferrate(II) complexes heated at 300°C for 3 h exhibit an asymmetric doublet, as shown in Figs. 1B and 2B, which may be further resolved into a quadrupole doublet ($\Delta E_Q = 0.89$ and 0.74 mm s^{-1} and $\delta = 0.13$ and 0.22 mm s^{-1}) and a singlet with $\delta = -0.05$ and -0.07 mm s^{-1} respectively. In di-*s*-butylamine-substituted complexes, both ΔE_Q and δ values are increased compared to those for room temperature. These may correspond to Fe(III) and Fe(II), both in low-spin state, presumably due to partial decomposition. In this process, water molecule and ligand may be released [17]. The weight loss shows complete removal of water molecules is supported by infrared spectra in which the intensity of the absorption band due to water molecule decreases as compared to that of cyanide. The removal of a coordinated water molecule changes the s-electron density at the iron nucleus. Dehydration of pentacyanoferrates(II) affects the crystal structure of the complexes without changing the cubic symmetry of the iron nucleus. The isomer shift of the potassium hexacyanoferrate(II) trihydrate increases on dehydration [28]. A similar trend is observed here.

When these complexes were heated at 400 and 500°C, a drastic change occurred as indicated by 7 lines with a singlet in the Mössbauer spectra (Figs. 1C, 1D, 2C and 2D). However, at 400°C the Mössbauer spectra are complex in di-*s*-Bu- and tri-*n*-Am-substituted pentacyanoferrates(II) and may be resolved into two set of sextets with $H_{eff} = 490$ and 457 kOe. These may correspond to the formation of Fe_3O_4 [28] along with $Fe(CN)_2$. As the temperature is increased to 700°C, magnetic phases containing a mixture of carbide and oxide start appearing. This is confirmed by the 2–3 sextets with $H_{eff} = 209, 460$ and 490 kOe respectively. At the still higher temperature of 800°C, a magnetic hyperfine splitting with a centrally located doublet is observed in the di-*s*-butylamine-substituted complex (Fig. 1G). This may be due to the formation of a mixture of α-Fe and magnetite (Fe_3O_4 (A) and Fe_3O_4 (B)). The doublet gives $\Delta E_Q = 0.46$ mm s^{-1} and $\delta = 0.37$ mm s^{-1} which may be attributed to α-$NaFeO_2$ [28] (Fig. 1G). In the case of the tri-*n*-amylamine-substituted complex, however, there is only the doublet with $\Delta E_Q = 0.46$ mm s^{-1} and $\delta = 0.36$ mm s^{-1} (Fig. 2G). This may be due to the α-$NaFeO_2$.

At 950°C, the Mössbauer spectrum is much resolved and displays the classical 12 lines of magnetite. This may be due to the population of both sites of the inverse spinel, the tetrahedral and the octahedral, superimposed with a haematite in both substituted complexes. The spectrum may be resolved into three sets of a sextet with $H_{eff} = 460, 490$ and 520 kOe (Fig. 1H and 2H). The Mössbauer spectrum of one of the end products is that of magnetite (Fe_3O_4) which is spinel ferrite $Fe^{3+}(Fe^{2+}Fe^{3+})O_4$. It has been reported that a fast electron transfer process take place between Fe^{2+} and Fe^{3+} ions at higher temperatures. However, at lower temperatures, the iron has discrete valence states and the material has an orthorhombic crystal structure. The temperature dependances of sites A (Fe^{3+}) and B (Fe^{2+}, Fe^{3+}) have been reported within the range 300–800 K [29].

3.4.2. Pyrazole-pyrrole- and pyrazine-substituted pentacyanoferrate(II)

Thermograms of pyrazole-, pyrazine- and pyrrole-substituted pentacyanoferrate(II) complexes yield 18.5, 16.0 and 24.0% residual weights respectively at ~950°C. The weight losses correspond to the formation of different iron species. Sileo et al. [17] also reported the formation of elemental iron and metal carbide. The pyrazole-substituted complex gives a DTG peak at 120°C, exhibiting slow decomposition upto 800°C and later it decomposes rapidy upto 1000°C. Beyond 1000°C it decomposes slowly. Thermograms of pyrazine- and pyrrole-substituted complexes show a multi-stage decomposition. In the pyrazine-substituted complex, four DTG peaks appear at 90, 230, 300 and 980°C exhibiting stepwise decomposition. For the pyrrole-substituted pentacyanoferrate(II) complex, three DTG peaks are observed at 120, 520 and 950°C.

Mössbauer spectra of pyrazole- and pyrrole-substituted complexes heated at 150°C for 3 h exhibit an asymmetrical doublet (Fig. 3B and 5B) with increased ΔE_Q of 0.78 and 0.85 mm s^{-1} respectively. This can be further resolved into a doublet with similar parameters and a singlet with a reduced δ value, suggesting partial decomposition. It seems that the state of the iron is formed in a somewhat symmetric environment. In the case of the pyrazine-substituted complex, only a slightly enhanced quadrupole doublet is obtained. This is further supported when the Mössbauer spectrum of the complexes heated at 300°C exhibit an asymmetrical doublet that can be resolved into a quadrupole doublet and a singlet (Figs. 3C, 4C and 5C). These may correspond to Fe(III) and Fe(II), both in a low-spin state, presumably due to partial decomposition. In this process, water molecule and ligand may be released [17]. At 500°C, pyrazole- and pyrazine-substituted complexes exhibit a complex spectrum with a central doublet with $\Delta E_Q = 0.58$ and 1.51 mm s^{-1} (Figs. 3D and 5D). The complex spectrum may be resolved into two sets of sextets with $H_{eff} = 490$ and 460 kOe suggesting the formation of magnetite. In the case of pyrrole, the magnetically split well-defined spectrum and its peak positions and the magnitude of the internal magnetic field are in good agreement with those reported in the literature [30]. The complex nature of the spectrum at 500°C can be attributed to the simultaneous presence of magnetite and haematite.

Subsequent heating at 600, 700, and 800°C yields a mixture of iron metal, metal carbide, magnetite and haematite. In the case of pyrazine-substituted complex heated at 600 and 700°C, complex spectra were obtained which may be due to the formation of iron carbide and iron metal (Figs. 5E, 5F). The spectrum at higher temperatures tallies

very closely with the spectrum reported for the cast iron superimposed by paramagnetic and ferromagnetic forms of cementite [31]. The pyrrole-substituted complex heated at 750°C exhibits a complex spectrum with a central doublet with $\Delta E_Q = 0.73$ mm s^{-1}. This spectrum may be resolved into four sextets with 209, 460, 488 and 331 kOe corresponding to the formation of Fe_3C, Fe_3O_4 (A and B) and α-Fe respectively. This is also supported by the XRD results.

In order to identify the end products of the complexes, these have been further heated at 950°C for 3 h. At 950°C, the pyrrole-substituted complex exhibits a sextet with magnetic hyperfine splitting ($H_{eff} = 492$ kOe) and a central doublet with $\Delta E_Q = 0.65$ mm s^{-1}. These may be due to the formation of γ-Fe_2O_3 and α-$NaFeO_2$ respectively. The XRD powder pattern of the pyrrole complex after heating at 950°C showed intense lines corresponding to the formation of γ-Fe_2O_3. In the case of the pyrazole-substituted complex, a six-line with central doublet is observed which gives $H_{eff} = 330$ kOe. This may correspond to the formation of iron metal and iron oxide. At 950°C for the pyrazine-substituted complex a six-line spectrum with $H_{eff} = 520$ kOe is observed which may be due to the formation of α-Fe_2O_3.

Acknowledgements

We are thankful to the Monbusho (Government of Japan) for awarding the fellowship to RBL and financial assistance for carrying out this work.

References

[1] P.J. Aymonino, M.A. Blessa, J.A. Olabe and E. Frank, Z. Naturforsch., 31B (1976) 1532.
[2] P.T. Manoharan and J.C. Fanning, J. Phys. Chem., 82 (1978) 1043.
[3] S.S.S. Borges, A.L. Coelho, I.S. Moreira and M.A.B. de Araujo, Polyhedron, 13 (1994) 1015.
[4] B.A. Narayanan and P.T. Manoharan, J. Inorg. Nucl. Chem., 40 (1978) 1993.
[5] H. Toma, J.A. Vanin and M.J. Malin, Inorg. Chim. Acta, 33 (1979) L157.
[6] J. Jwo, P.L. Gaus and A. Haim, J. Am. Chem. Soc., 101 (1979) 6189.
[7] H. Binder, Z. Anorg. Allg. Chem., 429 (1977) 247.
[8] A.L. Coelho, I.S. Moreira, J.H. de Araujo and M.A.B. de Araujo, J. Radioanal. Nucl. Chem. Lett., 136 (1989) 299.
[9] R.B. Lanjewar and A.N. Garg, Bull. Chem. Soc. Jpn., 64 (1991) 2502; Indian J. Chem., 34A (1995) 59.
[10] R.B. Lanjewar, Ph.D. Thesis, Nagpur University, Nagpur, 1991.
[11] D.V. Parwate and A.N. Garg, Z. Naturforsch, 40B (1985) 1495; Polyhedron, 5 (1986) 999.; J. Radioanal. Nucl. Chem. Lett., 87 (1984) 379.
[12] A.A. Batista, H.E. Toma and H.B. Gray, J. Am. Chem. Soc., 26 (1982) 104.
[13] M.M. Chamberlain and A.F. Greene, Jr., J. Inorg. Nucl. Chem., 25 (1963) 1471.
[14] J.I. Kunrath, C.S. Muller and E. Frank, J. Therm. Anal., 14 (1978) 253; An. Quim., 77 (1981) 307.
[15] L.A. Gentile, J.A. Olabe, E. Baran and P.J. Aymonino, J. Therm. Anal., 7 (1975) 279.
[16] A.S. Brar and S.P. Varma, Radiochem, Radioanal. Lett., 45 (1980) 45.
[17] E.E. Sileo, M.G. Posse, M.J. Morando and M.A. Blessa, Polyhedron, 6 (1987) 1757.
[18] F.A. Cotton, R.R. Manchamp, R.J.M. Henry and R.C. Vaung, J. Inorg. Nucl. Chem., 10 (1959) 28.
[19] P.T. Manoharan and H.B. Gray, J. Am. Chem. Soc., 87 (1965) 3340.
[20] H. Inoue, M. Sasagawa and E. Fluck, Z. Naturforsch., 40b (1985) 22.
[21] J.A. Olabe and P.J. Aymonino, J. Inorg. Nucl. Chem., 36 (1974) 1221; 38 (1976) 225.

[22] E. Fluck, H. Inoue, M. Nagao and S. Yanagisawa, J. Inorg. Nucl. Chem., 41 (1979) 287.
[23] H. Inoue, M. Sasagawa, E. Fluck and T. Shirai, Bull. Chem. Soc. Jpn, 56 (1983) 3434.
[24] D.P.E. Dickson and F.J. Berry, Mössbauer spectroscopy, Cambridge University Press, London, 1986.
[25] P. Gütlich, in U. Gonser (Ed.), Mössbauer spectroscopy, Springer, Heidelberg, 1975, p. 53.
[26] S. Ganguli and M. Bhattacharya, J. Chem. Soc. Faraday Trans., 79 (1983) 1513.
[27] H. Inoue, T. Nakazawa, T. Mitsuhashi, T. Shirai and E. Fluck, Hyperfine Interact. 46 (1989) 725.
[28] Y. Hazony, J. Chem. Phys., 45 (1966) 2664.
[29] F. Voued, G.A. Swatzky and A.H. Morrish, Phys. Rev., 167 (1968) 533.
[30] T. Birchall and N.N. Greenwood, *J. Chem. Soc.* A, 1969, 2382.
[31] M. Ron., H. Schechter, A.A. Hirsch and S.Niedzwiedz, Phys. Lett., 20 (1960) 481.